Received: 2 August 2021 | Revised: 21 February 2022 | Accepted: 14 March 2022
DOI: 10.1002/qj.4271

Quarterly Journal of the Royal Meteorological Society RMetS

RESEARCH ARTICLE

Observing severe precipitation near complex topography during the Yilan Experiment of Severe Rainfall in 2020 (YESR2020)

Shih-Hao Su[1] | Yu-Hung Chang[2] | Ching-Hwang Liu[1] | Wei-Ting Chen[2] | Wei-Yu Chang[3] | Jen-Ping Chen[2,4] | Wei-Nai Chen[5] | Kao-Sheng Chung[3] | Jou-Ping Hou[6] | Min-Ken Hsieh[2,7] | Yi-Shin Jang[2] | Hung-Chi Kuo[2] | Yu-Chi Lee[7] | Pay-Liam Lin[3] | Ping-Yu Lin[7] | Po-Hsiung Lin[2,4] | Min-Hui Lo[2,4] | Sheng-Hsiang Wang[3] | Chien-Ming Wu[2] | Jing-Hwa Yang[1] | Ming-Jen Yang[2]

[1]Department of Atmospheric Sciences, Chinese Culture University, Taipei, Taiwan

[2]Department of Atmospheric Sciences, National Taiwan University, Taipei, Taiwan

[3]Department of Atmospheric Sciences, National Central University, Taoyuan, Taiwan

[4]International Degree Program in Climate Change and Sustainable Development, National Taiwan University, Taipei, Taiwan

[5]Research Center of Environmental Change, Academia Sinica, Taipei, Taiwan

[6]Department of Environmental Information and Engineering, Chung Cheng Institute of Technology, National Defense University, Taoyuan, Taiwan

[7]Central Weather Bureau, Taipei, Taiwan

Correspondence
W.-T. Chen, Department of Atmospheric Sciences, National Taiwan University, Taipei, Taiwan.
Email: weitingc@ntu.edu.tw

Funding information
Ministry of Science and Technology, Taiwan, Grant/Award Numbers: MOST-108-2119-M-002-022, MOST-110-2123-M-002-007, MOST109-2628-M-002-003-MY3

Abstract
This study introduces a recent field experiment investigating multiscale terrain–circulation–precipitation interactions. When a synoptic-scale northeasterly wind prevails under the active East Asian winter monsoon, stratocumulus cloud decks with severe rainfall exceeding 100 mm·day^{-1} frequently occur in the northeastern plain area and adjacent mountains in Yilan, Taiwan. The Yilan Experiment of Severe Rainfall (YESR2020) is a field campaign from November 20, 2020, to November 24, 2020, to survey the physical processes leading to severe wintertime rainfall. The three-dimensional structure of the wind field and the atmospheric environment can be identified through high temporal and spatial resolution sounding observations, which is empowered by the novel Storm Tracker mini-radiosonde. During YESR2020, the continuously collected meteorological data of two northeasterly episodes captured the variability of local-scale wind patterns and the features of the severe rainfall induced by stratocumulus. A preliminary analysis indicated that a local-scale convergence line could appear over the plain area of Yilan under the northeasterly environmental condition. The precipitation hotspot was located in the mountain region of southern Yilan, where the local winds signified turbulence features. Moreover, the severe rainfall of the two northeasterly episodes spotlighted shallow cumulus under stratus with pure warm rain processes. The results of YESR2020 inspire the arrangement of future field observations to explore detailed mechanisms of heavily precipitating stratocumulus over complex topography.

KEYWORDS
heavily precipitating stratocumulus, Storm Tracker mini-radiosonde, terrain–circulation–precipitation interactions, Yilan Experiment of Severe Rainfall

1 INTRODUCTION

Marine stratocumulus clouds have been intensively studied as they are recognized to play a critical role in modulating the radiative balance of the climate system (Stephens and Greenwald, 1991; Hartmann *et al.*, 1992; Stephens, 2005). Previous investigations of precipitation processes in marine stratocumulus have been mainly focused on the formation of drizzle and light rain associated with the changes in cloud microphysics and dynamics, predominantly for the persisting low cloud decks over the northeastern and southeastern Pacific (Wood, 2012). Over the northwestern Pacific, where the East Asian winter monsoon is active, transient marine stratocumulus clouds are formed in the regions where the near-surface northeasterly monsoonal wind is enhanced by the synoptic systems (Koike *et al.*, 2012; Koike *et al.*, 2016; Liu *et al.*, 2016; Chang, Chen, and Chen, 2021; Wu and Chen, 2021), as shown in the example in Figure 1a. With the presence of the marine stratocumulus, the boundary layer is moistened through enhanced vertical mixing (Lilly, 1968). The combination of the prevailing northeasterly monsoonal wind and the moist cloud-topped boundary layer can provide strong and steady low-level horizontal moisture flux approaching the terrain of Taiwan, which is likely a critical environment for heavy precipitation to be generated in the windward coastal mountains and the plains, particularly in Yilan.

The wintertime averaged accumulated precipitation in Yilan is about 200–1,200 mm, with frequent episodes of severe rainfall exceeding 100 mm·day^{-1} (Figure 1b). Typically, the duration of severe rainfall events in wintertime in Yilan is about 20–60 hr. Over the mountain region of southern Yilan, where the highest average rainfall and the greatest frequency of severe rainfall events occur, the rain rate is mostly around 10–20 mm·hr^{-1}, with a maximum of about 50 mm·hr^{-1}. These regular and ample wintertime rainfall events guarantee the water resources for both the socioeconomic activities and the unique cloud forest ecosystem in the mountains of northeastern Taiwan. The severe rainfall events also lead to flash floods, trigger landslides, and damage major highways. Chen *et al.* (1980) and Lee and Chen (1983) identified how the synoptic-scale weather patterns modulated the regional precipitation in several severe wintertime rainfall cases in northern Taiwan. However, the discussions on local precipitation characteristics were limited due to the lack of high-resolution field observations and numerical models in the early days. The features of stratocumulus producing heavy precipitation and their interactions with the terrain were also not investigated.

Many previous studies show that orographic-induced precipitation is highly related to background flow and mountain geometry (e.g., Imamovic *et al.*, 2019). The primary theoretical mechanism emphasizes the mechanical lifting of moist unstable air masses (Houze, 2012), which could cause precipitation in the windward side of the mountains. However, heavy winter rainfall in Yilan occurred not only in the mountain region but also over the plain area. By summarizing pilot balloon, surface wind, and precipitation observations in Yilan in December 1942, Kabasawa (1950) suggested that the variability of the northeasterly background environment and its interactions with the terrain can influence the local wind field. Such a concept can be extended to the interactions between the large-scale circulation field and the orographic-generated small-scale turbulence. The turbulence generated by the terrain may increase the vertical mixing in the planetary boundary layer (PBL) and alter the structure of the stratocumulus, which can likely enhance the precipitation intensity locally. Therefore, heavy precipitation in Yilan is potentially a phenomenon caused by the cross-scale interactions over the terrain, which requires a dense array of sounding observations to resolve the local circulation.

Several field campaigns have been carried out in recent years aiming at the terrain–convection–precipitation interactions. The Convective and Orographically induced Precipitation Study was operated in a low-mountain area in Europe in the summertime (Wulfmeyer *et al.*, 2011), collecting the observations with multiple instruments covering the entire evolution of convective precipitation events over the terrain. The Remote Sensing of Electrification, Lightning, and Mesoscale/Microscale Processes with Adaptive Ground Observations field campaign in the summertime in South America highlighted the high-impact deep convection along with complex topography (Nesbitt *et al.*, 2021). The Olympic Mountains Experiment in the wintertime in Washington State revealed how precipitation is modified by the terrain (Houze *et al.*, 2017). Recently, some field experiments also focused on the interactions between the terrain and regional circulation under a relatively dry atmospheric environment. The Perdigão field campaign in the summertime utilized high-density devices to monitor the near-surface wind turbulence over complex topography in Portugal. They pointed out that the near-surface fine-scale wind features can be captured by suitable remote-sensing instruments, such as lidar, radar, and ceilometer, over a very complex topography (Fernando *et al.*, 2019; Bell *et al.*, 2020). Compared with these previous field experiments, the severe wintertime rainfall in Yilan occurs in a relatively cooler and more humid environment with higher potential instability, and Taiwan has a steeper and higher orographic regime.

In the past 40 years, several joint observational experiments have been held in Taiwan. Most investigations

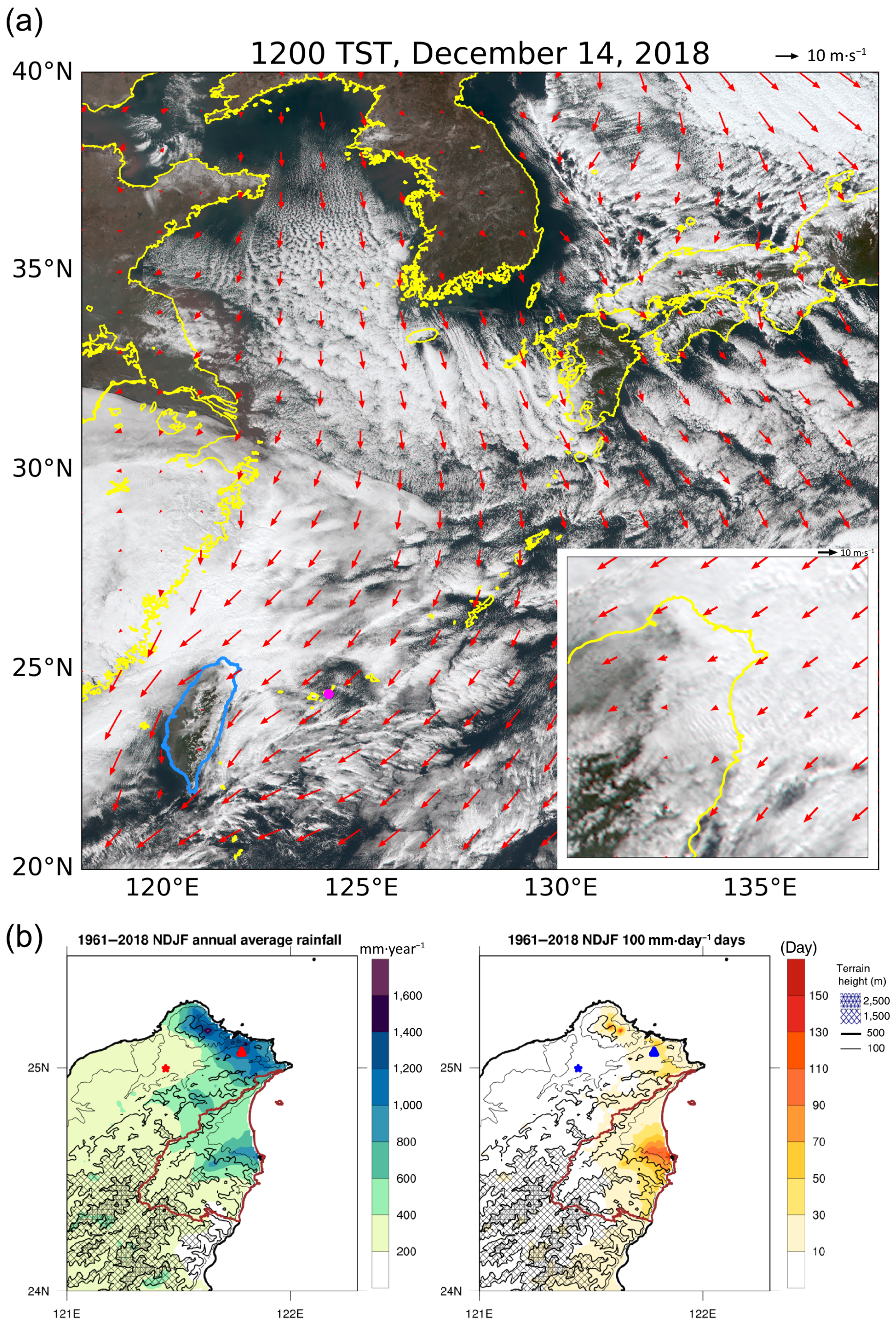

FIGURE 1 (a) True-color image by Himawari-8 (Takenaka *et al.*, 2020; Yamamoto *et al.*, 2020) and 10 m wind of the fifth generation of the European Centre for Medium-Range Weather Forecasts atmospheric reanalysis (ERA5; Hersbach *et al.*, 2020) at 1200 h Taiwan standard time (TST, UTC + 8) December 14, 2018, over East Asia during a severe rainfall event in the northeastern part of the Taiwan Island (outlined in blue). In this severe case, the 48-hr accumulated rainfall at Suaou reached 445.0 mm with the maximum hourly rainfall being 27.5 mm. The dot is Ishigaki Island. (b) The climatology (1961–2018) of accumulated precipitation (left) and the frequency of severe rainfall events (right) during the wintertime (November–February, NDJF) in northeastern Taiwan. The thick line shows the boundary of Yilan County. The triangular mark is the location of the Central Weather Bureau (CWB) Wufenshan operational radar, and the star is the location of the CWB Banqiao sounding site [Colour figure can be viewed at wileyonlinelibrary.com]

focused on the high-impact synoptic-scale weather events in the warm season, including the Taiwan Area Mesoscale Experiment (Kuo and Chen, 1990) in 1987 and the Southwest Monsoon Experiment (Jou *et al.*, 2011) in 2008. Some regional experiments were focused on precipitation and convection-related topics, such as the Green Island Mesoscale Experiment (Jou, 2001) in 2001 and the Taipei Summer Storm Experiment (TASSE; Kuo *et al.*, 2017) in the late 2010s. In Taiwan, the interactions between terrain, circulation, and precipitation in the wintertime environment have never been observed with modern equipment of high spatial and temporal frequency.

The Central Weather Bureau (CWB) established the automatic surface observational network covering the mountain region in Taiwan. It provided continuous measurements of temperature, humidity, wind, rainfall, and radiation (only a few sites) at the surface (Figure 2a). However, the variability of low-level wind can only be captured with frequent sounding observations within the PBL, which are not feasible with the two existing operational upper-air sounding stations in Taiwan Island. Moreover, convection and precipitation over complex topography can also modulate the local circulation. Thus, the internal structures of stratocumulus and the detailed evolution of

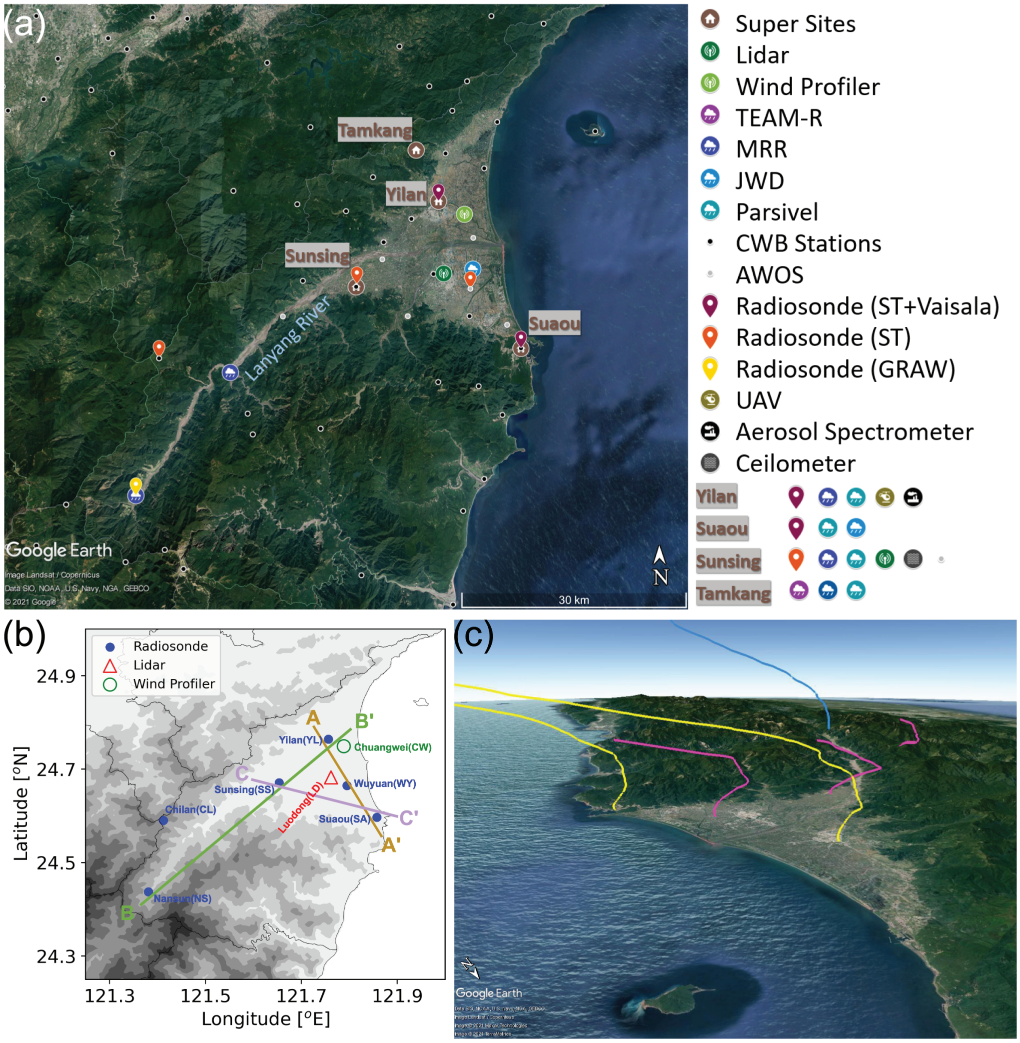

FIGURE 2 (a) Instrumental placement during the Yilan Experiment of Severe Rainfall in 2020. (b) The sites with upper-level wind observations. The dots, triangle, and circle are the sites for radiosondes, lidar, and wind profiler, respectively. Three cross-section lines are chosen to analyze the vertical structure of the wind field: the coast line (A–A′, Suaou–Wuyuan–Luodong–Chuangwei–Yilan), the valley line (B–B′, Nansan–Sunsing–Yilan–Chuangwei), and the southern line (C–C′, Sunsing–Luodong–Wuyuan–Suaou). (c) The three-dimensional trajectories of storm trackers were released from six observational sites in the Yilan area at 0800 h Taiwan standard time (UTC + 8) November 24. Each site provides a vertical profile of the moisture, temperature, and wind fields. Satellite photographs are captured from Google Earth. AWOS, automated weather observing system; CWB, Central Weather Bureau; JWD, Joss–Waldvogel disdrometer; MRR, micro rain radar; ST, Storm Tracker; TEAM-R, Taiwan Experimental Atmospheric Mobile Radar; UAV, uncrewed aerial vehicle [Colour figure can be viewed at wileyonlinelibrary.com]

precipitation are also critical information to be obtained. Therefore, a carefully designed high-frequency, fine-scale observational array covering different parts of the terrain to measure winds in the PBL, cloud, and rainfall is critical to resolving the terrain–circulation–precipitation interactions.

In 2020, we carried out an intensive field campaign, Yilan Experiment of Severe Rainfall (YESR2020), to understand the interactions between terrain, circulation, and precipitation in the wintertime in Yilan using state-of-the-art instruments. An array that can observe the three-dimensional wind field was constructed using the Storm Tracker mini-radiosonde (Hwang *et al.*, 2020), wind profiler, and wind lidar. The sounding observations provide not only the structure of the wind field but also the vertical profiles of the thermodynamic features. We also deployed an X-band precipitation radar of 3 cm wavelength, micro rain radars (MRRs), and raindrop size disdrometers to monitor the cloud evolution. YESR2020 is the first modern campaign that focuses on the local circulation associated with severe rainfall in winter in Taiwan since World War II.

The primary objectives of this article are to introduce the field campaign design of the YESR2020 and to present the preliminary analyses on the local-scale wind fields and rainfall observed by the network of the Storm Tracker mini-radiosonde and remote-sensing instruments during the major episodes under northeasterly synoptic conditions with severe rainfall. The article is organized as follows. The deployment plan and the instruments are described in Section 2. The synoptic weather evolution during the campaign period is reviewed in Section 3. The preliminary analysis for local circulation during two main rainfall events is shown in Section 4. Discussion on the results and the potential scientific topics associated with YESR2020 are presented in Sections 5 and 6, respectively.

2 | DEPLOYMENT PLAN AND INSTRUMENTATION LIST

2.1 | Deployment plan

The YESR2020 field campaign was designed to observe the evolution of precipitation patterns, PBL turbulence, and three-dimensional circulation characteristics during periods with northeasterly monsoonal wind encountering complex topography. The intensive observing period (IOP) was November 20–24, 2020. Within this joint field campaign framework, an extensive suite of the state-of-the-art meteorological instrument and advanced micro-observational equipment were operated concurrently for the first time in Yilan. Five institutions were involved in this field campaign. Various additional instruments were deployed over the plain area of Yilan to enhance the observations of the low-level kinematic and microphysical data of precipitation systems. The network is comprised of instruments for in-situ measurements, including a high temporal and spatial resolution automated weather observing system and active remote-sensing instruments, such as advanced radar and lidar systems. Meanwhile, we also collect PBL data through drone sounding and particulate matter (PM) observations. We had 16 additional stations in Yilan with 30 CWB surface stations (Figure 2a). All types of instruments operated during YESR2020 are listed in Table 1, including their supporting institutions, available parameters, and operating sites.

Figure 2 shows the spatial deployment of the instruments, which were orientated across (northwest to southeast, coast line, A–A′ in Figure 2b) and along (northeast to southwest, valley line, B–B′ in Figure 2b) the Lanyan River. The instruments along the Lanyan River provide northeasterly monsoonal wind characteristics, including the wind speed, wind direction, instability,

TABLE 1 The list of instruments operated during the Yilan Experiment of Severe Rainfall in 2020

Instrument	Institution[a]	Parameter	Site
Lidar	RCEC	Wind profile	Luodong
	NDUCCIT	Wind profile	Sunsing
Wind profiler	NCU	Wind profile	Chuangwei
TEAM-R[b]	NCU	Radial velocity, radar reflectivity, differential reflectivity, correlation coefficient, differential phase shift	Tamkang
MRR/MRR-pro	NTU, NCU, PCCU	Vertical-pointing radar reflectivity, raindrop fall speed	Yilan, Sunsing, Tamkang, Nansun, Tuchang
JWD	PCCU, NCU	Raindrop size distribution	Suaou, Wujie
Parsivel	PCCU	Raindrop size distribution	Yilan, Suaou, Sunsing, Tamkang
Aerosol spectrometer	NTU	Aerosol size distribution	Yilan
Ceilometer	NTU	Cloud base height	Sunsing
UAV	NCU	Temperature, humidity, pressure, wind speed, wind direction, $PM_{2.5}$ mass concentration	Yilan

[a]NCU, National Central University; NDUCCIT, Chung Cheng Institute of Technology, National Defense University; NTU, National Taiwan University; PCCU, Chinese Culture University; RCEC, Research Center for Environmental Change, Academia Sinica.
[b]Taiwan Experimental Atmospheric Mobile Radar (TEAM-R) operation was available only during November 20–21, whereas all the other instruments were operating during the whole intensive observing period.
Abbreviations: JWD, Joss–Waldvogel disdrometer; MRR, micro rain radar; PM, particulate matter; UAV, uncrewed aerial vehicle.

and kinematic and microphysical structures. Moreover, the cross-orientated instruments provide local circulation characteristics induced by surrounding mountains. Furthermore, the past observational experiments on the initiation process of convection in the terrain indicated that the variables of PBL moisture, local circulation, and rainfall are significantly related to the frequency of convection initiation (Weckwerth and Parsons, 2006). Therefore, we also set up several sounding sites along the southern mountains (southern line, C–C′ in Figure 2b). The sounding network can provide detailed information on meso-γ-scale low-level circulation variations for the terrain-related return flow over the plain area of Yilan. These high temporal and spatial sounding observations can sufficiently and effectively observe the environmental characteristics of the PBL, which are helpful to the study of the orographic precipitation mechanism. They are also crucial for the ground-truth validation of the high-resolution large-eddy simulation (LES) model and remote-sensing retrievals.

2.2 | Instrumentation

2.2.1 | Radiosonde

The sounding observations provide the most reliable atmospheric pressure, temperature, and humidity measurements. However, currently, there is no operational sounding site in Yilan, with the closest operational sounding site being located in the Taipei basin (the star in Figure 1b). As Taipei is on the opposite side of the mountain range, it cannot provide the crucial PBL characteristics in Yilan for this study. Therefore, we need to release numerous radiosondes during the IOP to observe the three-dimensional atmospheric environment with a high spatial and temporal resolution.

During YESR2020, we took advantage of the previous experiment of TASSE, which systematically carried out the co-launch of the Storm Tracker mini-radiosonde (Figure 3; Hwang *et al.*, 2020) with the operational Vaisala radiosonde, providing a suitable calibration reference for the Storm Tracker mini-radiosonde. Table 2 shows the frequency and duration of radiosonde release. At the supersites (Yilan and Suaou), we carried out a co-launch procedure similar to TASSE. Furthermore, using the Storm Tracker mini-radiosonde can increase the frequency and coverage of observations. In addition, the GRAW radiosonde was also utilized during YESR2020, providing atmospheric status upstream of the Lanyang River. The concurrent radiosonde release as a network at six sites (Figure 2c) provides the vertical environmental conditions and detailed information of low-level microscale turbulence (Luce and Hashiguchi, 2020) in Yilan.

2.2.2 | Wind field remote sensing

Although the environmental wind conditions can be obtained from the sounding observations, extra vertical-pointing wind profilers and wind lidars were operated during YESR2020 to improve spatial and temporal observational resolution. By deploying very high frequency and vertical-pointing remote-sensing measurements, we can greatly enhance the ability to resolve the wind conditions in Yilan. The variation of

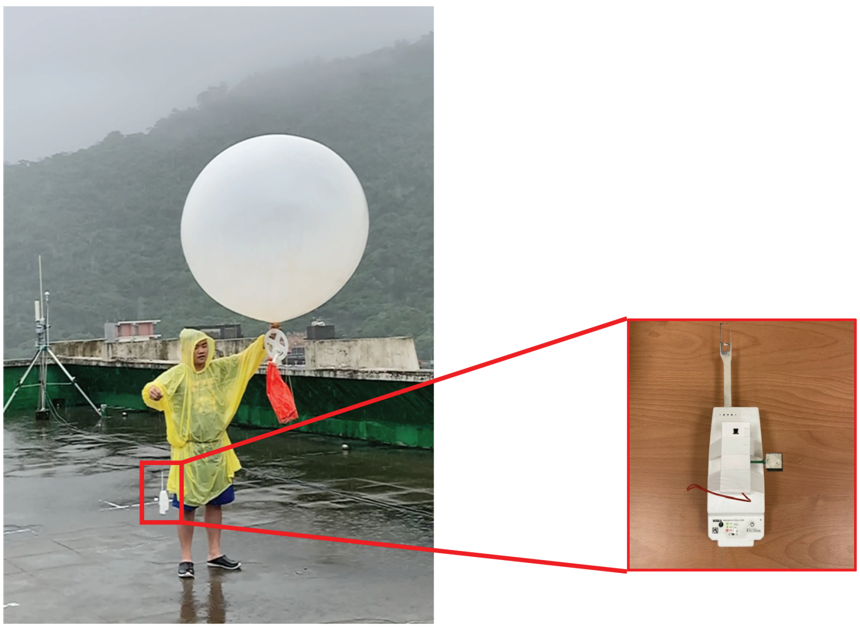

FIGURE 3 Co-launch of the Storm Tracker mini-radiosonde with the operational Vaisala RS41-SGP radiosonde during the Yilan Experiment of Severe Rainfall in 2020 [Colour figure can be viewed at wileyonlinelibrary.com]

TABLE 2 The frequency and duration of radiosonde release during the Yilan Experiment of Severe Rainfall in 2020

Sounding site	Elevation (m)	Radiosonde system	Release frequency
Yilan	8.4	Storm Tracker (co-launch with Vaisala RS41-SGP)	Every 3 hr (co-launch every 6 hr before 1400 h TST (UTC + 8) November 23, and every 3 hr after that)
Suaou	24.9		
Sunsing	80.0	Storm Tracker	Every 3 hr
Wuyuan	37.9		
Chilan	1,711.0	Storm Tracker	Every 1.5 hr during the daytime, and every 3 hr during the nighttime[a]
Nansun	1,260.0	GRAW	Every 6 hr

[a]Daytime is 0500–2000 h Taiwan standard time (TST; UTC + 8), and nighttime is 2000–0500 h TST (UTC + 8).

wind conditions is essential to understand the developing mechanism of precipitation systems.

2.2.3 | Radar

Owing to the altitude limitation and orographic-blocking issue, the low-level (below 1 km) precipitation characteristics cannot be well observed by the CWB operational radar at Wufenshan (the triangle on Figure 1b). Therefore, the Taiwan Experimental Atmospheric Mobile Radar (TEAM-R; Chang *et al.*, 2014) was deployed during YESR2020. The X-band polarimetric radar measurements examined the cloud dynamical structures and microphysical characteristics of convective precipitation systems at high spatial and temporal resolution (every 7.5 min and 1.0 km^2). The hybrid-scanning strategy of TEAM-R contains the plan position indicator (PPI) volume scans, vertical scan, and the range height indicator scans. The elevation angles of the PPI scans were 0.5, 1.0, 2.0, 3.0, 4.0, 5.0, 6.0, 7.0, 8.5, 10.5, 15.0, and 19.5°. Meanwhile, the azimuthal angles of the range height indicator scan were strategically selected and regularly repeated over the location of MRRs to consistently obtain detailed vertical microphysical characteristics of precipitation systems. MRRs can provide profiles of raindrop size distribution and Doppler velocity of falling raindrops. The fall velocity observed by MRRs can be utilized to differentiate ice crystals and aggregated dendrites as they have distinct fall velocities. Therefore, the structure of the clouds can be verified by MRRs, illustrating the state of the hydrometeors.

2.2.4 | Microphysics observations

Several instruments were operated during YESR2020 to obtain further information on cloud microphysical processes. The laser aerosol spectrometer (GRIMM 1.109), which can provide airborne PM number concentration of 31 size channels between 0.25 and 32 μm, was installed at Yilan station. The size distribution of the aerosols can provide further information focusing on aerosol activation and warm-rain physical processes. The modern particle size and velocity optical disdrometer (Parsivel) and Joss–Waldvogel disdrometers can profile the raindrop size distribution and terminal velocity information for all types of precipitating events during YESR2020. The raindrop information were associated with the observations from five vertical-pointing MRRs during this period. In addition, TEAM-R provided high spatiotemporal resolution of dual-polarimetric measurements for retrieving raindrop size distribution and differentiating hydrometer types of precipitation systems.

2.2.5 | Uncrewed aerial vehicle

In YESR2020, we also used an innovative automatic quadcopter system to observe meteorological and air quality conditions in the lower troposphere. YESR2020 is the first time this uncrewed aerial vehicle (UAV) system operated simultaneously with radiosondes during a joint field campaign. Our UAV system has customized features, including being waterproof and having high wind resistance (up to 17 m·s^{-1}) and low form drag, which allows us to operate it in severe weather. The UAV was equipped with meteorological and $PM_{2.5}$ sensors to obtain the vertical distribution of temperature, humidity, pressure, wind speed, wind direction, and $PM_{2.5}$ mass concentration. We operated a total of 17 vertical profiling flights at Yilan station, aiming to conduct the intercomparison between the UAV and the operational Vaisala radiosonde. The maximum flight height of the UAV was 2,500 m. The UAV ascent rate was set at 3.5 m·s^{-1}, and the data were recorded at 1 s resolution.

3 | SYNOPTIC WEATHER EVOLUTION

The IOP period of the YESR2020 field campaign was November 20–24 in Yilan. The evolution of the synoptic weather, the radar quantitative precipitation estimation, and the background northeasterly moisture transport profiles calculated using the Ishigaki Island (about 230 km east of Yilan; the magenta dot in Figure 1a) operational sounding observations are presented in Figure 4. We identify a northeasterly episode when the low-level northeasterly moisture transport intensifies within 12 hr. During the IOP period of YESR2020, two northeasterly episodes occurred.

On the morning of November 20, a cold front was located to the northeast of Taiwan (the left column of Figure 4a). As the cold front passed through, the low-level northeasterly moisture transport surged (the right column of Figure 4a), signifying the beginning of the first northeasterly episode. On November 21, the low-level northeasterly moisture transport weakened in the evening, marking the termination of the first northeasterly episode (the right column of Figure 4b). The surface wind speed at Ishigaki Island remained weaker than 8.2 m·s^{-1} during the whole episode. It precipitated in northeastern Taiwan during the whole episode, and the most significant precipitation hotspot was in the mountain region of southern Yilan (the middle columns in Figure 4a,b).

The left column of Figure 4c shows that there were no primary synoptic weather systems around Taiwan on November 22, and the isobars were sparse. At this time, the center of the continental cold high-pressure system was located in Mongolia and its edge was at the coast of China. During the daytime, the northeasterly moisture transport was low, and the precipitation occurred mainly in the northeastern tip of Taiwan.

The second northeasterly episode started on the evening of November 22, at which the northeasterly moisture transport increased (right column of Figure 4c). The left column of Figure 4d demonstrates that the isobars around Taiwan became more compact on November 23. On November 24, the center of the continental cold high-pressure system moved southward to central China (left column of Figure 4e). The surface wind speed at Ishigaki Island was consistently greater than 7.7 m·s^{-1} during the whole episode, with a maximum of 10.8 m·s^{-1}, which is more intense than that in the first episode. The most significant precipitation hotspot was again the mountain region of southern Yilan (middle columns in Figure 4d,e). This northeasterly episode proceeded and settled until November 25.

The Himawari-8 geostationary satellite true-color images (Figure 4f) show that well-developed marine stratocumulus clouds were embedded in the regions of near-surface strong northeasterly monsoonal wind that extended from the upstream ocean to northeastern Taiwan in both northeasterly episodes when severe rainfall events occurred over Yilan. The formation of marine stratocumulus cloud decks indicated that the marine atmospheric boundary layer exhibited high moisture and sufficient vertical mixing for condensation. The low-level moisture could be transported by the prevailing northeasterly winds and served as the water vapor source of the severe rainfall events in Yilan. As shown in the right columns of Figure 4a,d, the peak values of the northeasterly moisture transport almost reached 180 g·kg^{-1}·m·s^{-1}. These high moisture transport values indicated that the synoptic-scale northeasterly continuously supplied water vapor in the low-level atmosphere towards northeastern Taiwan, which was a favorable ambient condition for severe rainfall events.

Figure 5a illustrates the evolution of PBL moisture and horizontal wind observed by the three-hourly released Storm Tracker mini-radiosonde at Yilan station. The frequent sampling revealed that the atmospheric characteristics at Yilan station were locally and swiftly transitioned. Note that the low-level water vapor observed at Yilan station during the first northeasterly episode (November 21) was higher than during the second episode (November 23–24). The local water vapor in the PBL could be influenced by small-scale processes, such as local circulation transport, convective mixing, and precipitation evaporation. The precise high spatial and temporal resolution observations are essential to fully understand the severe rainfall and its relationship with the local-scale atmospheric phenomenon in Yilan. Figure 5b further demonstrates that the performance of the calibrated Storm Tracker mini-radiosonde in the lower atmosphere is comparable to the Vaisala RS41-SGP radiosonde, which is the sensor used in current CWB daily operational sounding observations. The characteristics of the atmospheric environment in the PBL can be accurately observed by the Storm Tracker mini-radiosonde, which enables the following of local-scale analysis of fine-resolution atmospheric profiles.

4 | TWO NORTHEASTERLY EPISODES WITH SEVERE RAINFALL

The two northeasterly episodes with severe rainfall during YESR2020 had a similar synoptic weather system layout. Although the mountain region of southern Yilan was the most significant precipitation hotspot in both northeasterly episodes, the detailed characteristics of precipitation and local wind field were different. The sounding

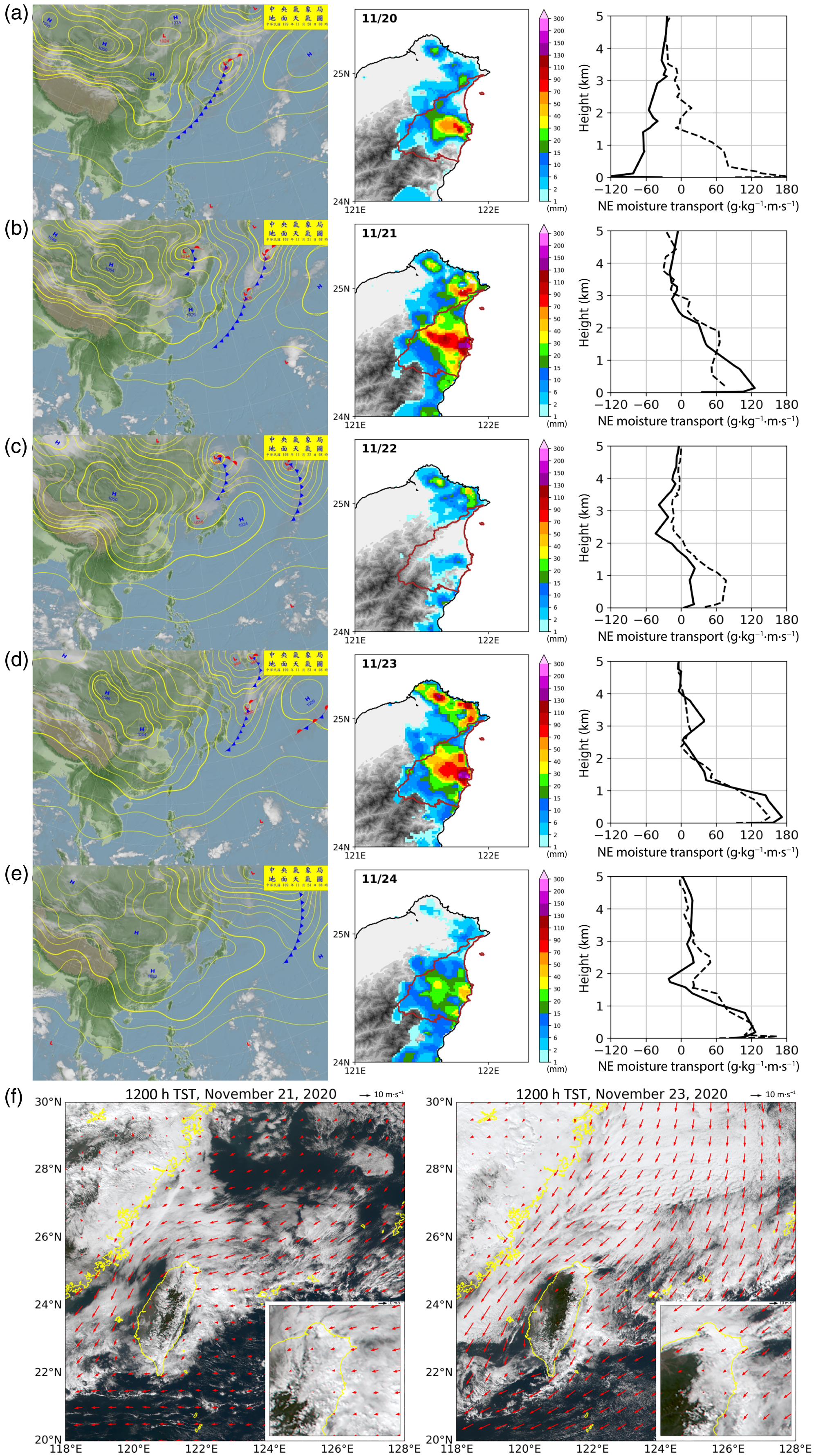

FIGURE 4 (a–e) Synoptic weather charts at 0800 Taiwan standard time (TST; UTC + 8) from the Central Weather Bureau (CWB) are presented in the left column. Radar quantitative precipitation estimation daily accumulated rainfall from the CWB is displayed in the middle column. The northeasterly (NE) moisture transport calculated using sounding observations at 0800 h TST (UTC + 8; solid line) and 2000 h TST (UTC + 8; dashed line) November 20–24 at Ishigaki Island is shown in the right column. (f) Himawari-8 true-color image and ERA5 10 m wind at 1200 h TST (UTC + 8) November 21 and 1200 h TST (UTC + 8) November 23 [Colour figure can be viewed at wileyonlinelibrary.com]

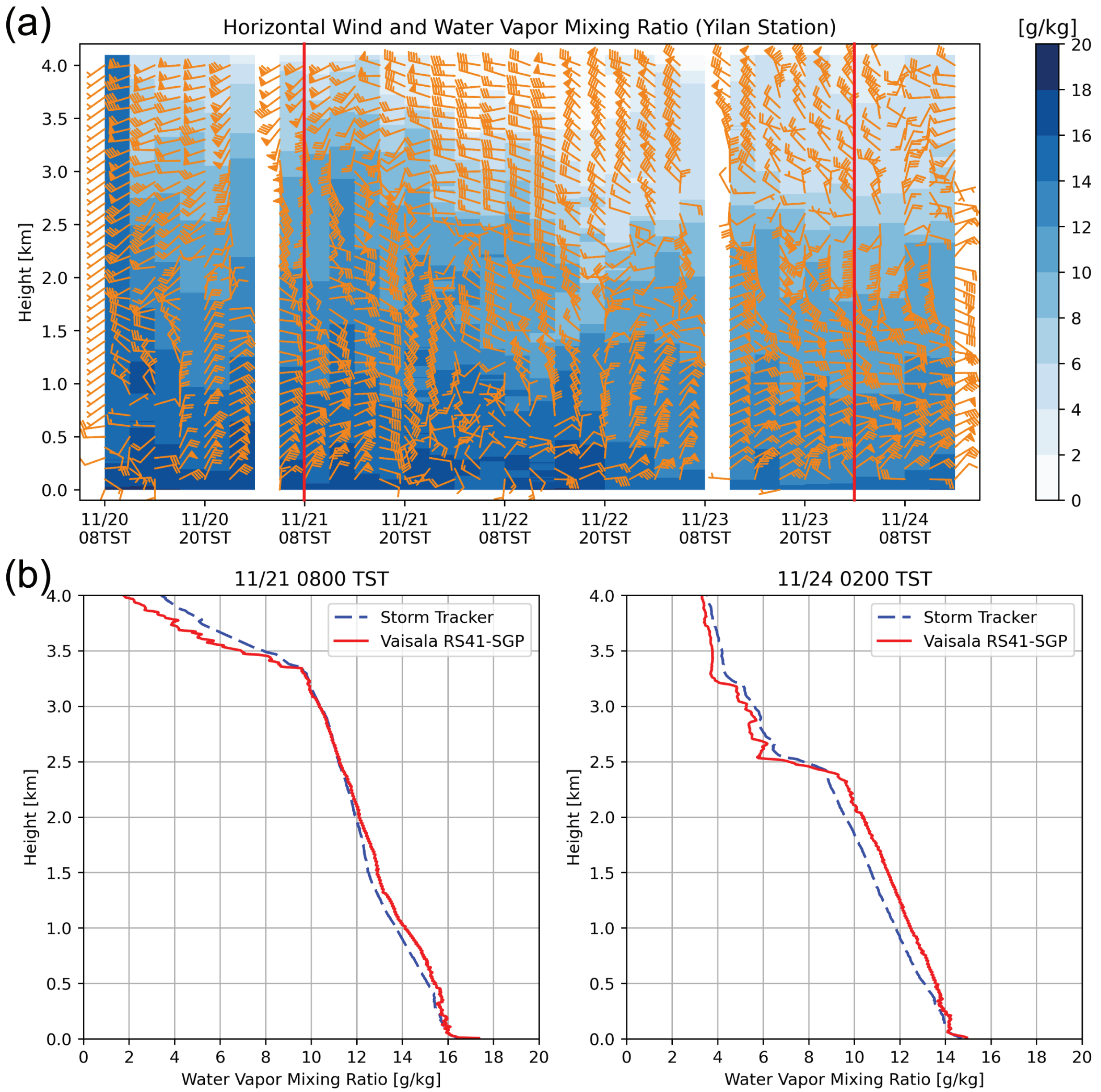

FIGURE 5 (a) Time evolution of water vapor mixing ratio and horizontal wind below 4 km (planetary boundary layer) at Yilan station during the Yilan Experiment of Severe Rainfall in 2020. One full wind barb represents 2 m·s^{-1}. The boxes represent the period of two northeasterly episodes. (b) Comparison of observed water vapor mixing ratio between the Vaisala RS41-SGP radiosonde (solid lines) and the Storm Tracker mini-radiosonde (dashed lines) at 0800 h Taiwan standard time (TST; UTC + 8) November 21 (during the first episode) and 0200 h TST (UTC + 8) November 24 (during the second episode) [Colour figure can be viewed at wileyonlinelibrary.com]

observations and the wind field remote sensing could be applied to construct the detailed structures of the regional PBL circulation variations, enabling us to distinguish the two episodes by their features of low-level wind fields.

The first northeasterly episode began in the daytime of November 20 and terminated on the evening of November 21. Figure 6 shows that the northeasterly flow generally prevailed over the plain area during the whole episode, consistent with the background synoptic wind pattern. The surface wind field turned northeasterly at 0800 h Taiwan standard time (TST; UTC + 8) November 20, but not until 1700 h TST (UTC + 8) November 20 did the precipitation initiate over the plain area of Yilan. The heavy rain rate of more than 10 mm·hr^{-1} emerged from 2000 h TST (UTC + 8) November 20 in the mountain region of southern Yilan and its adjacent plain area. The heavy rain rate area expanded northward and peaked at 1400 h TST (UTC + 8) November 21. Soon after, the wind direction turned southeasterly, and the precipitation weakened at 1700 h TST (UTC + 8) November 21. The 48-hr accumulated rainfall was 230.5 mm, 66.0 mm, and 33.5 mm at Suaou, Sunsing, and Yilan

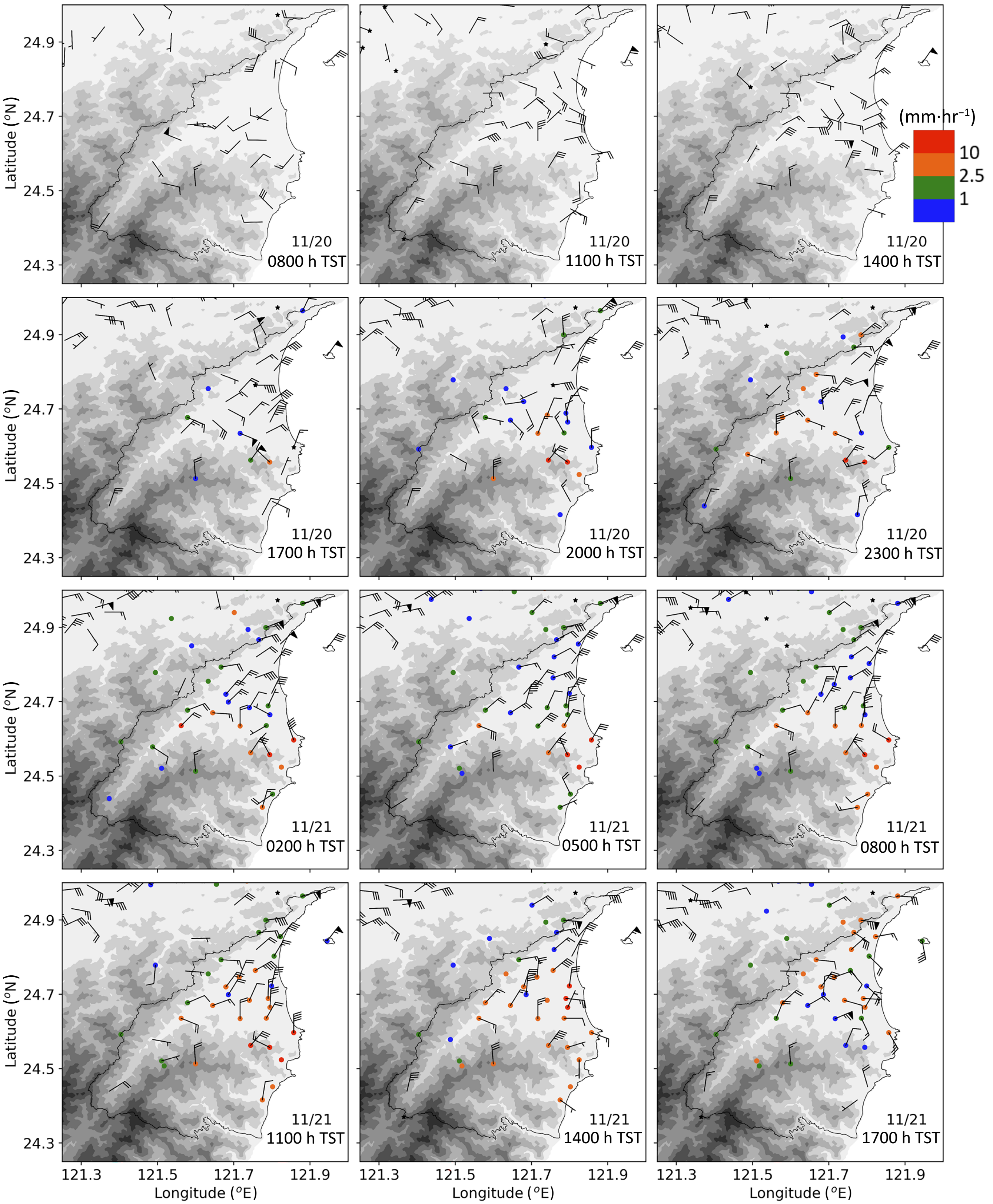

FIGURE 6 Evolution of horizontal wind and precipitation pattern at the surface during November 20–21. The stars mark missing rainfall data. One full wind barb represents 1 $m \cdot s^{-1}$. The surface observational data were obtained from the automated weather observing system established by the Central Weather Bureau and provided by the observational teams of the Yilan Experiment of Severe Rainfall in 2020 [Colour figure can be viewed at wileyonlinelibrary.com]

stations, respectively. The severe precipitation occurred in the mountain region of southern Yilan, and the precipitation decreased northward over the plain area. Figure 7 demonstrates a two-layer horizontal wind structure during the first episode. The three cross-section lines bear similar time evolutions of the wind profile features. The upper-level westerly flow, a typical wintertime synoptic feature in Taiwan (Chen and Chen, 2003), and the low-level easterly flow evolved with time, relating to the progress of the synoptic-scale northeasterly monsoonal wind. The low-level easterly flow mainly existed below 1,000 m at 1400 h TST (UTC + 8) November 20, and it thickened and reached about 3,000 m in the next 24 hr. Furthermore, a turbulent feature could be found below the upper-level westerly flow at the sounding stations in the southern line of Figure 7, identified qualitatively through the vertically varying horizontal wind.

The polarimetric X-band TEAM-R observations further provided the microphysical structure and the rain properties inside the cloud decks over the plain area of Yilan to the coastal ocean during the first episode. Figure 8 shows TEAM-R's systematic bias and attenuation-corrected measurements (Chen *et al.*, 2021). Based on the reflectivity Z_{HH} and differential reflectivity Z_{DR}, the height of the convection top was less than 6 km during this period (Figure 8a,b). There was no bright-band signature, implying that the convection was entirely below the freezing level. The values of Z_{DR} were around 0.2–1.2, indicating the mean drop size was small. The correlation coefficient ρ_{HV} values were between 0.9 and 1.0 (Figure 8c), suggesting that the pure warm-rain droplets were uniform and small. This heavy precipitation system features a shallow convective system with pure warm-rain processes. The interactions between the local circulation, the cloud development, and the terrain that lead to severe precipitation in Yilan will be the primary focus of future studies.

The second northeasterly episode started on the evening of November 22 and proceeded until November 25. The 48-hr accumulated rainfall at Suaou, Sunsing, and Yilan stations was 167.5 mm, 84.5 mm, and 44.5 mm, respectively. Although the mountain region of southern Yilan was still the most significant precipitation hotspot, the total amount was lower than that during the first episode. Contrasting with the first episode, Figure 9 reveals that the surface wind field over the plain area of Yilan did not completely correspond to the background synoptic northeasterly pattern. The wind field over the inland part of the plain area was westerly, while easterly to northeasterly flow appeared over the coastal side of the plain area. Thus, a clear convergence line appeared over the plain area. Note that the precipitation over the plain area of Yilan was not centered around the convergence line. The convergence line shifted northward during 0500–1400 h TST (UTC + 8) November 23, and the rain rate increased for the stations to the south of the convergence line. The position of the convergence line was variable between 2000 h TST (UTC + 8) November 23 and 0200 h TST (UTC + 8) November 24, which was the period that the heaviest rainfall occurred in the mountain region of southern Yilan in this northeasterly episode. The location of the convergence line was relatively fixed from 0200 h TST (UTC + 8) November 24. Figure 10 displays the horizontal wind structure along the three cross-section lines during the second episode. A near-surface westerly flow emerged beneath the low-level easterly flow, different from the first episode. Generally speaking, Suaou and Wuyuan in the coast line and Sunsing in the valley line had deeper near-surface westerly flow. These sites were located near the mountains of southern Yilan, indicating that the near-surface westerly flow could be related to the terrain. As the near-surface westerly flow evolved, its structure along the coast line and the valley line remained relatively steady; the near-surface westerly flow was thicker to the south and shallower to the north. However, its structure temporally varied along the southern line. The depth of the near-surface westerly flow thickened to the west and decreased to the east with time. Turbulence near the mountain region of southern Yilan was also displayed in the sounding observations of Sunsing and Wuyuan below the interface of the northeasterly monsoonal wind and the upper-level westerly flow (southern line in Figure 10). This characteristic was different from the conceptual model proposed by Kabasawa (1950) and will be discussed in the next section.

5 | DISCUSSION

A field campaign was conducted in Yilan in late December 1942 to investigate the mechanism of the wintertime orographic precipitation (Kabasawa, 1950). Pilot balloons were released at three sites and seven additional surface observational sites of wind and precipitation were established over the plain area of Yilan. Kabasawa's summary schematics (redrawn in Figure 11a) revealed that the surface wind field over the inland part of the plain area was westerly, whereas easterly to northeasterly flow appeared over the coastal side of the plain area. Precipitation mainly occurred along a convergence line that appeared over the plain area. Over the inland part of the plain area, the cloud cover was scattered, and there was no rainfall. The cloud top of stratocumulus clouds was lower than 2,000 m. It was postulated that when the northeasterly monsoonal wind encountered the terrain the mechanical

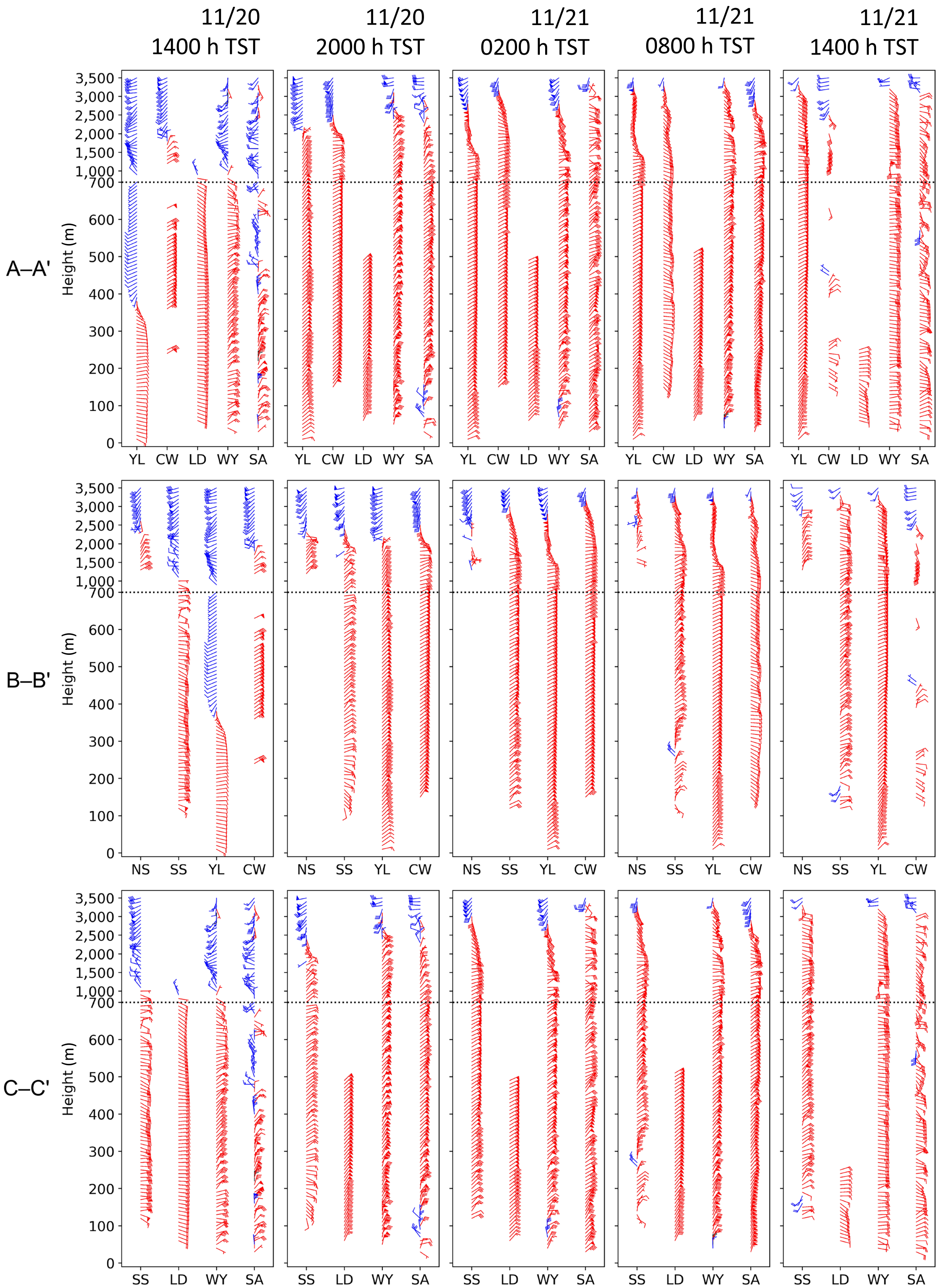

FIGURE 7 Evolution of vertical cross-sections of horizontal winds during November 20–21. One full wind barb represents 2 m·s^{-1}. Vertical resolution is 25 m below 1,500 m and 100 m above 1,500 m. TST, Taiwan standard time (UTC + 8) [Colour figure can be viewed at wileyonlinelibrary.com]

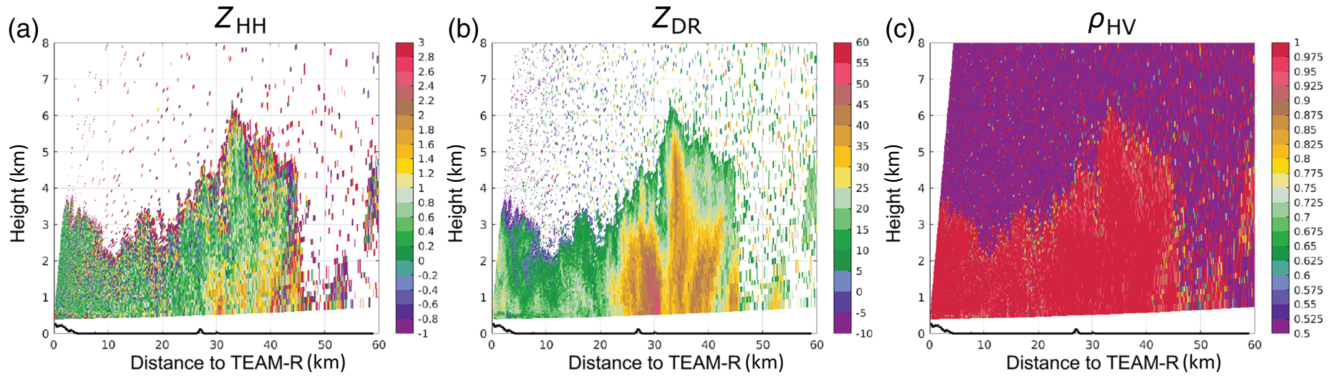

FIGURE 8 The range height indicator scan of (a) reflectivity Z_{HH}, (b) differential reflectivity Z_{DR}, and (c) correlation coefficient ρ_{HV} observed by Taiwan Experimental Atmospheric Mobile Radar at an azimuth angle of 152° during the first northeasterly episode at 0407 h Taiwan standard time (TST; UTC + 8) November 21. The black, solid line represents the terrain height [Colour figure can be viewed at wileyonlinelibrary.com]

blocking caused stable subsidence and the near-surface southwesterly return flow.

Based on the high-resolution sounding observations and modern remote-sensing instruments, we summarize the terrain–circulation–precipitation interactions during the second episode of YESR2020 in Figure 11b. We discovered that a convergence line appeared over the plain area of Yilan. The variability of the convergence line could be related to the background monsoonal wind and the orographic precipitation. The mountain region of southern Yilan was the precipitation hotspot, and the areas with precipitation greater than 2.5 mm·hr^{-1} were limited to the south of the convergence line (Figure 9). In other words, the precipitation maxima did not occur along the convergence line. The spatial arrangement of the local wind field and precipitation indicate that the formation of the near-surface westerly flow likely involves other processes, such as a precipitation-induced cold pool or cold air drainage by surface radiative cooling along with the terrain instead of the mechanically induced flow. Moreover, the cloud top of stratocumulus clouds was around 3,000 m with the thickness around 2,500 m, indicating more water content for stratocumulus and a higher chance of severe precipitation. The horizontal wind profile at Sunsing and Wuyuan showed the development of turbulence and considerable rainfall (84.5 mm in 48 hr) near the mountain region of southern Yilan.

The local wind field structure observed during the second episode of YESR2020 was similar to that in Kabasawa (1950) above the scale of around 20 km, showcasing the characteristics of the convergence line. However, the detailed structure of the horizontal wind profile indicated that the phenomenon and the physical processes were different from that proposed by Kabasawa (1950). The advanced observational instruments enabled us to precisely resolve the wind field and the microphysical features in a wintertime severe rainfall event. From our observations, we postulate that the orographic-induced local turbulence is the critical pivot relating to the severe rainfall in the mountain region and over the plain area near the mountains. The complex regional terrain–circulation–precipitation interactions can play a critical role in maintaining the rainfall intensity and efficiency. Thus, further investigations will be carried out to untangle the dominating physical processes, especially the roles of environmental dynamic and thermodynamic conditions, cloud dynamics, and the PBL turbulence over the complex topography.

6 | SUMMARY AND OUTLOOK

The YESR2020 field campaign assembled a rich array of sounding observations with the novel Storm Tracker mini-radiosonde for PBL profiling systems. The goal of YESR2020 is to understand the variability of local circulation associated with the unique wintertime severe rainfall events when the upstream northeasterly monsoonal wind, accompanied with the formation of marine stratocumulus, encounters the complex topography in Yilan, Taiwan. Aside from the wind profile observations, the ground-based remote sensing on cloud and precipitation enables us to construct a first-order conceptual model of cross-scale turbulent interactions between the prevailing wind and the orographic-induced return flow. We note that although the synoptic-scale weather patterns in the two northeasterly episodes were similar they had very different regional features during YESR2020. Overall, the large-scale background wind field was roughly northeasterly during these two periods, and the precipitation hotspots were both in the mountain region of southern Yilan. However, the two episodes' local-scale horizontal

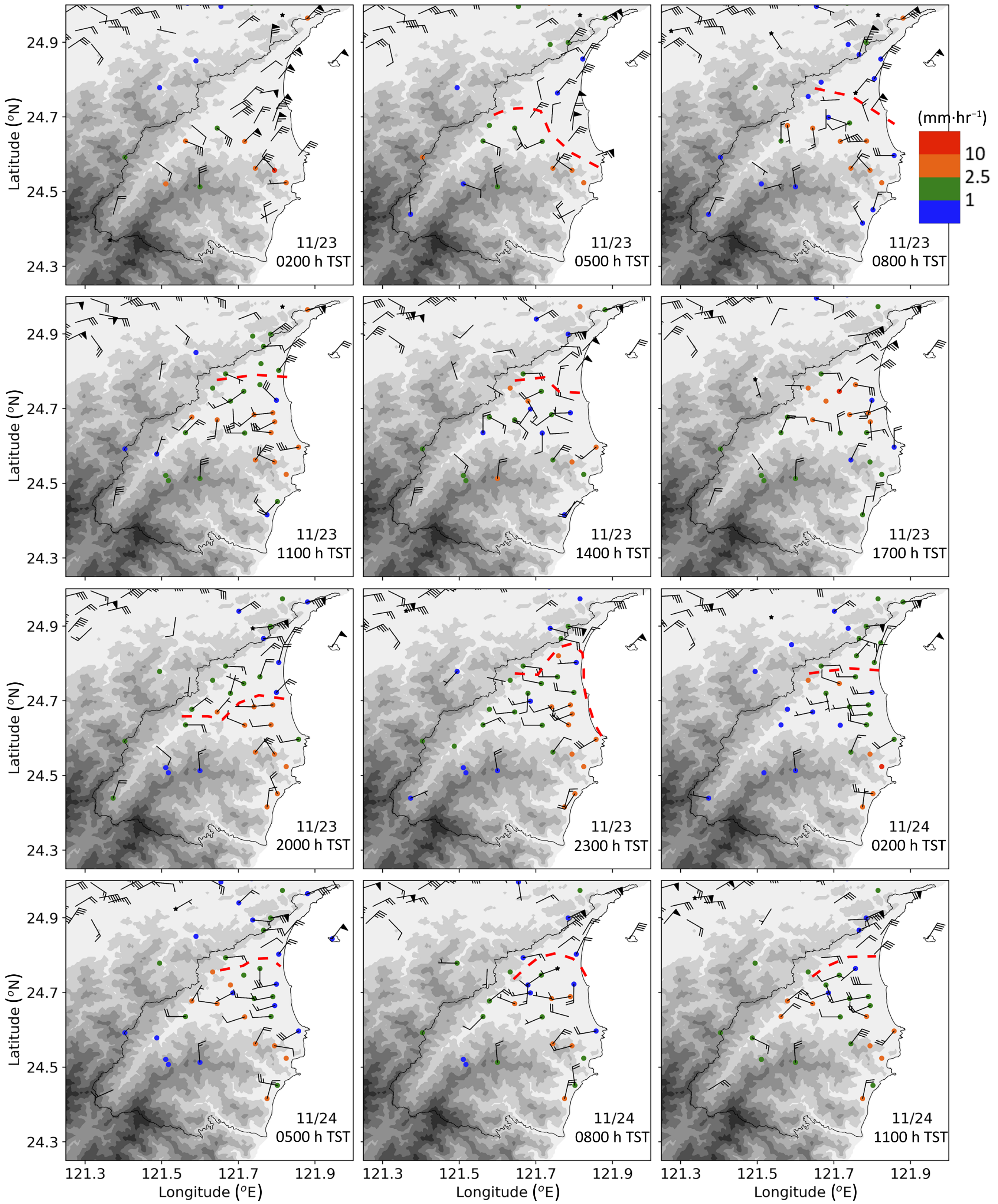

FIGURE 9 Same as Figure 6, except during November 23–24. The dashed lines represent the convergence lines [Colour figure can be viewed at wileyonlinelibrary.com]

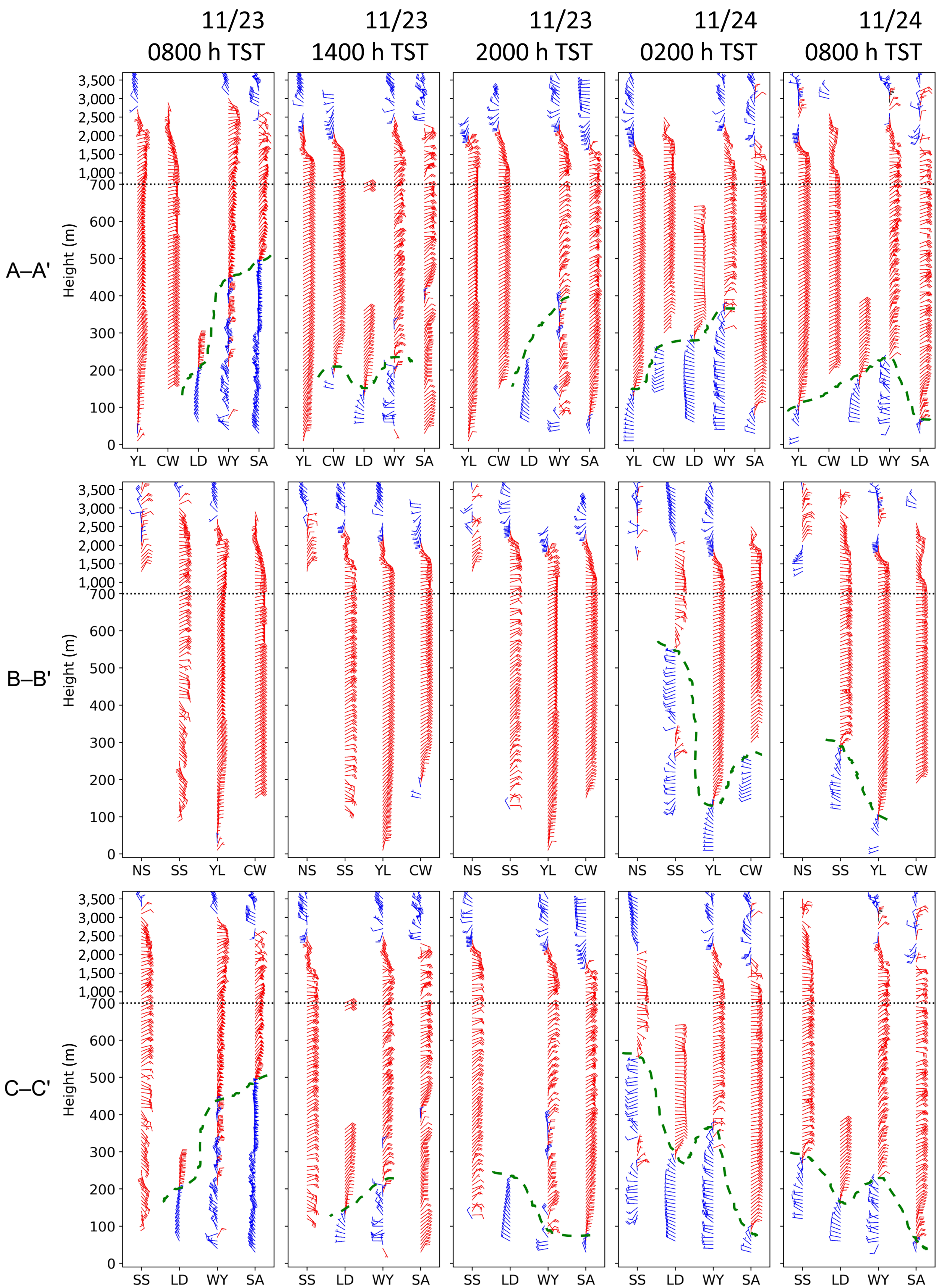

FIGURE 10 Same as Figure 7, except during November 23–24. The green dashed line represents the interface of the near-surface westerly flow and the northeasterly monsoonal wind [Colour figure can be viewed at wileyonlinelibrary.com]

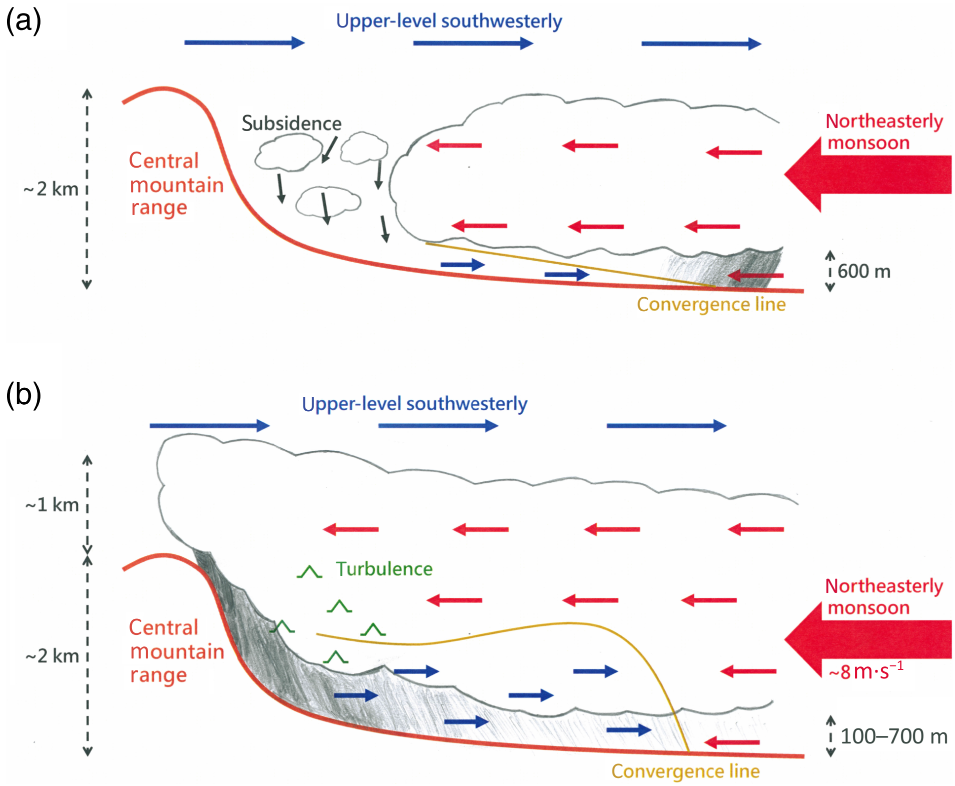

FIGURE 11 (a) Schematics redrawn from Kabasawa (1950). (b) Schematics of severe rainfall in Yilan, based on the observations during the second northeasterly episode of the Yilan Experiment of Severe Rainfall in 2020. The triangles represent turbulence, and the gray shading displays the degree of rain rate. The strength of the background northeasterly monsoonal wind is based on the wind speed around 900 hPa at Ishigaki Island [Colour figure can be viewed at wileyonlinelibrary.com]

wind and precipitation patterns can be distinguished. Over the plain area of Yilan, the surface wind field was northeasterly during the first episode, whereas a clear convergence line appeared during the second episode. Meanwhile, a larger precipitation contrast between the mountain region and the plain area of Yilan was found in the first episode, indicating a more significant spatial variation of rainfall.

In the future, high-resolution model simulations will be applied to examine the physical processes and untangle the causal relationship. For example, idealized or semi-realistic LESs using the vector vorticity equation model with high-resolution (500 m) realistic terrain of the Taiwan island (TaiwanVVM; Wu *et al.*, 2019; Chang, Chen, Wu, *et al.*, 2021) can resolve the local wind pattern and the properties of clouds and precipitation. This model framework can represent the crucial physical processes in the PBL, enabling the interactions between the background environment, the orographic-related wind pattern, and the severe rainfall. Thus, the influence of the background wind variation on severe local rainfall in Yilan could be clarified by performing systematic sensitivity experiments. Figure 12 shows the surface wind field simulated by TaiwanVVM under different northeasterly directions with a low moisture background condition. In this case, the drier atmosphere prohibited the precipitation formation, allowing the examination of the local circulation development without the interference of precipitation formation. We noticed that the simulated local circulation is sensitive to the direction of low-level background wind, as the local surface wind patterns are distinctively different when the initial upstream wind direction changes from more northerly (20°) to northeasterly (50°) and more easterly (80°). In the future, simulations with increasing background moisture will be performed to examine the evolution of precipitation development and its interactions with the local circulation. Under this simulation setting, and given sufficient simulation domain size, marine stratocumulus clouds can be formed in the upstream areas in the high-resolution LES. Thus, we will be able to examine the evolution of the vertical mixing depth and mixing efficiency in the PBL of upstream marine stratocumulus under different background flow patterns and moisture structures and their association with the downstream orographic-induced local wind and severe rainfall in Yilan.

Both the observations during YESR2020 and the TaiwanVVM simulation illustrate that the surface wind field near the terrain can be highly variable along the southern mountains of Yilan. A future YESR will focus on turbulence and its relationship with heavily precipitating stratocumulus. The Storm Tracker mini-radiosonde, combining the advantages of light weight and high vertical resolution, can be utilized in the mobile sounding observations to measure low-level turbulence (Ko *et al.*, 2019) induced by the terrain–circulation–precipitation interactions with great flexibility. In a future YESR, the

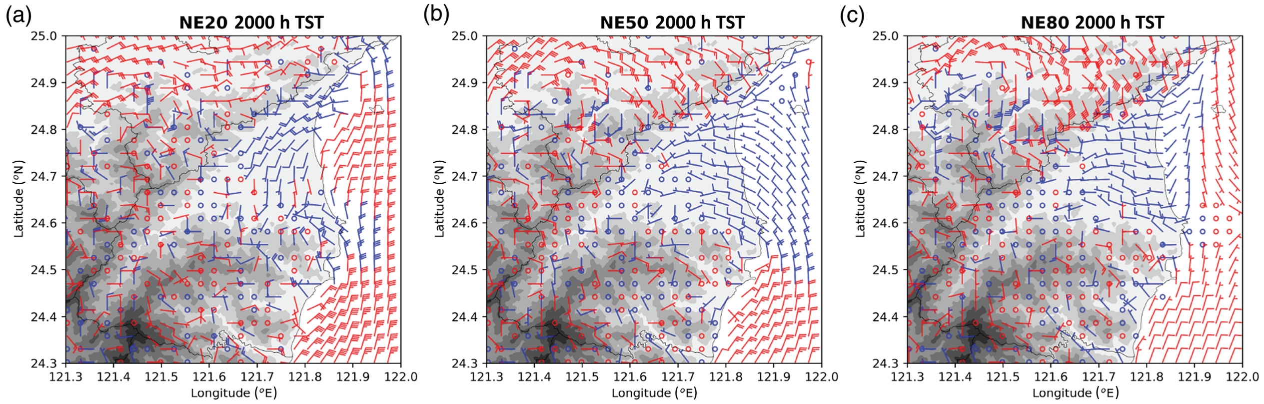

FIGURE 12 Surface wind field of Yilan area in TaiwanVVM simulations at 2000 h Taiwan standard time (TST; UTC + 8). The initial background wind directions are (a) 20°, (b) 50°, and (c) 80°. One full wind barb represents 2 m·s^{-1} [Colour figure can be viewed at wileyonlinelibrary.com]

cooperative observations of the radiosondes and the radar will pivot on turbulence related to heavily precipitating stratocumulus over complex topography.

The broad coverage of satellite observations can potentially be helpful to study the transition of marine stratocumulus encountering the coastal mountain terrain that produces heavy precipitation. However, the warm cloud phenomenon challenges satellite rainfall retrievals (Maranan *et al.*, 2020). As warm rain processes mainly produce the precipitation in the low cloud, the infrared-based rainfall retrievals are prone to underestimation because of the low contrast in the brightness temperatures between the cloud top and the surface. The space-borne radar can also underestimate surface rain rates as the near-surface reflectivity can be interfered with by surface clutter, particularly over the complex topography. The high temporal and spatial resolution ground-based observations during YESR2020 and the upcoming YESR campaign in the future will provide valuable measurements to systematically validate the satellite rainfall products from the plain area to the mountain region, leading to improvements of rainfall retrievals for this unique precipitation regime in the East Asian winter monsoon.

ACKNOWLEDGMENTS

This research was supported by the Taiwan Ministry of Science and Technology through grants MOST-108-2119-M-002-022, MOST109-2628-M-002-003-MY3, and MOST-110-2123-M-002-007. We sincerely thank all the staff, research assistants, and students who participated in the YESR2020 field campaign for measurements, logistics, and administrative work. We would also like to show our gratitude to the CWB for providing the observational venues, synoptic weather diagnoses, and ground-station data during YESR2020. We thank Tamkang University, which provided a suitable site for radar observations at Lanyang Campus. We thank the Data Bank for Atmospheric and Hydrologic Research (DBAR) for providing the observational data archive service during the field campaign. The YESR2020 data can be accessed via the DBAR (https://dbar.pccu.edu.tw/) after a 2-yeas data protection period. The Himawari 8/9 gridded data are distributed by the Center for Environmental Remote Sensing, Chiba University, Japan (ftp://hmwr829gr.cr.chiba-u.ac.jp/). We thank the Taiwan Climate Change Projection and Information Platform project for providing the gridded precipitation data. We sincerely thank Peng-Jen Chen for producing Figures 1a and 4f, Chiao-Wei Chang for producing Figure 1b, and Jun-Jie Chang for producing Figure 12.

AUTHOR CONTRIBUTIONS

Shih-Hao Su: Conceptualization; data curation; funding acquisition; investigation; methodology; resources; supervision; validation; writing – original draft; writing – review and editing. **Yu-Hung Chang:** Conceptualization; data curation; formal analysis; investigation; methodology; validation; visualization; writing – original draft; writing – review and editing. **Ching-Hwang Liu:** Conceptualization; data curation; investigation; methodology; project administration; resources; supervision; validation. **Wei-Ting Chen:** Conceptualization; funding acquisition; investigation; methodology; resources; supervision; writing – original draft; writing – review and editing. **Wei-Yu Chang:** Data curation; formal analysis; funding acquisition; investigation; methodology; resources; supervision; visualization; writing – review and editing. **Jen-Ping Chen:** Investigation; resources; software. **Wei-Nai Chen:** Data curation; investigation; resources; supervision. **Kao-Sheng Chung:** Data curation; funding acquisition; investigation; methodology; resources; supervision. **Jou-Ping Hou:** Data curation; investigation;

resources; supervision. **Min-Ken Hsieh:** Data curation; formal analysis; investigation. **Yi-Shin Jang:** Data curation; investigation. **Hung-Chi Kuo:** Conceptualization; data curation; funding acquisition; investigation; methodology; project administration; resources; supervision; writing – review and editing. **Yu-Chi Lee:** Resources; supervision. **Pay-Liam Lin:** Data curation; investigation; resources; supervision. **Ping-Yu Lin:** Data curation; formal analysis. **Po-Hsiung Lin:** Data curation; investigation; resources; supervision. **Min-Hui Lo:** Data curation; funding acquisition; investigation; methodology; resources; supervision; writing – review and editing. **Sheng-Hsiang Wang:** Data curation; funding acquisition; investigation; methodology; resources; supervision; writing – review and editing. **Chien-Ming Wu:** Conceptualization; data curation; funding acquisition; methodology; resources; software; writing – review and editing. **Jing-Hwa Yang:** Data curation; investigation; validation. **Ming-Jen Yang:** Data curation; software.

ORCID

Wei-Ting Chen https://orcid.org/0000-0002-9292-0933
Kao-Sheng Chung https://orcid.org/0000-0003-1459-7242
Min-Hui Lo https://orcid.org/0000-0002-8653-143X
Sheng-Hsiang Wang https://orcid.org/0000-0001-9675-3135

REFERENCES

Bell, T.M., Klein, P., Wildmann, N. and Menke, R. (2020) Analysis of flow in complex terrain using multi-Doppler lidar retrievals. *Atmospheric Measurement Techniques*, 13(3), 1357–1371. https://doi.org/10.5194/amt-13-1357-2020.

Chang, C.-W., Chen, W.-T. and Chen, Y.-C. (2021) Susceptibility of East Asian marine warm clouds to aerosols in winter and spring from co-located A-train satellite observations. *Remote Sensing*, 13(24), 5179.

Chang, W.-Y., Vivekanandan, J. and Chen Wang, T.-C. (2014) Estimation of X-band polarimetric radar attenuation and measurement uncertainty using a variational method. *Journal of Applied Meteorology and Climatology*, 53(4), 1099–1119. https://doi.org/10.1175/jamc-d-13-0191.1.

Chang, Y.-H., Chen, W.-T., Wu, C.-M., Moseley, C. and Wu, C.-C. (2021) Tracking the influence of cloud condensation nuclei on summer diurnal precipitating systems over complex topography in Taiwan. *Atmospheric Chemistry and Physics*, 21(22), 16709–16725. https://doi.org/10.5194/acp-21-16709-2021.

Chen, C.-S. and Chen, Y.-L. (2003) The rainfall characteristics of Taiwan. *Monthly Weather Review*, 131(7), 1323–1341. https://doi.org/10.1175/1520-0493(2003)131<1323:Trcot>2.0.Co;2.

Chen, G.T.-J., Lee, C.-W. and Liu, K.-Y. (1980) A primary study of abnormal rainfall over northern Taiwan under the northeast monsoon influence in winter season. *Atmospheric Sciences*, 7(1), 73–84 (in Chinese with English abstract).

Chen, J.-Y., Chang, W.-Y. and Chang, P.-L. (2021) A synthetic quantitative precipitation estimation by integrating S- and C-band dual-polarization radars over northern Taiwan. *Remote Sensing*, 13(1), 154. https://doi.org/10.3390/rs13010154.

Fernando, H.J.S., Mann, J., Palma, J., Lundquist, J.K., Barthelmie, R.J., Belo-Pereira, M., Brown, W.O.J., Chow, F.K., Gerz, T., Hocut, C.M., Klein, P.M., Leo, L.S., Matos, J.C., Oncley, S.P., Pryor, S.C., Bariteau, L., Bell, T.M., Bodini, N., Carney, M.B., Courtney, M.S., Creegan, E.D., Dimitrova, R., Gomes, S., Hagen, M., Hyde, J.O., Kigle, S., Krishnamurthy, R., Lopes, J.C., Mazzaro, L., Neher, J.M.T., Menke, R., Murphy, P., Oswald, L., Otarola-Bustos, S., Pattantyus, A.K., Rodrigues, C.V., Schady, A., Sirin, N., Spuler, S., Svensson, E., Tomaszewski, J., Turner, D.D., van Veen, L., Vasiljević, N., Vassallo, D., Voss, S., Wildmann, N. and Wang, Y. (2019) The Perdigão: peering into microscale details of mountain winds. *Bulletin of the American Meteorological Society*, 100(5), 799–819. https://doi.org/10.1175/BAMS-D-17-0227.1.

Hartmann, D.L., Ockert-Bell, M.E. and Michelsen, M.L. (1992) The effect of cloud type on Earth's energy balance: global analysis. *Journal of Climate*, 5(11), 1281–1304. https://doi.org/10.1175/1520-0442(1992)005<1281:TEOCTO>2.0.CO;2.

Hersbach, H., Bell, B., Berrisford, P., Hirahara, S., Horányi, A., Muñoz-Sabater, J., Nicolas, J., Peubey, C., Radu, R., Schepers, D., Simmons, A., Soci, C., Abdalla, S., Abellan, X., Balsamo, G., Bechtold, P., Biavati, G., Bidlot, J., Bonavita, M., De Chiara, G., Dahlgren, P., Dee, D., Diamantakis, M., Dragani, R., Flemming, J., Forbes, R., Fuentes, M., Geer, A., Haimberger, L., Healy, S., Hogan, R.J., Hólm, E., Janisková, M., Keeley, S., Laloyaux, P., Lopez, P., Lupu, C., Radnoti, G., de Rosnay, P., Rozum, I., Vamborg, F., Villaume, S. and Thépaut, J.-N. (2020) The ERA5 global reanalysis. *Quarterly Journal of the Royal Meteorological Society*, 146(730), 1999–2049. https://doi.org/10.1002/qj.3803.

Houze, R.A. (2012) Orographic effects on precipitating clouds. *Reviews of Geophysics*, 50(1), RG1001. https://doi.org/10.1029/2011RG000365.

Houze, R.A., McMurdie, L.A., Petersen, W.A., Schwaller, M.R., Baccus, W., Lundquist, J.D., Mass, C.F., Nijssen, B., Rutledge, S.A., Hudak, D.R., Tanelli, S., Mace, G.G., Poellot, M.R., Lettenmaier, D.P., Zagrodnik, J.P., Rowe, A.K., DeHart, J.C., Madaus, L.E., Barnes, H.C. and Chandrasekar, V. (2017) The Olympic Mountains Experiment (OLYMPEX). *Bulletin of the American Meteorological Society*, 98(10), 2167–2188. https://doi.org/10.1175/bams-d-16-0182.1.

Hwang, W.-C., Lin, P.-H. and Yu, H. (2020) The development of the "Storm Tracker" and its applications for atmospheric high-resolution upper-air observations. *Atmospheric Measurement Techniques*, 13(10), 5395–5406. https://doi.org/10.5194/amt-13-5395-2020.

Imamovic, A., Schlemmer, L. and Schär, C. (2019) Mountain volume control on deep-convective rain amount during episodes of weak synoptic forcing. *Journal of the Atmospheric Sciences*, 76(2), 605–626. https://doi.org/10.1175/JAS-D-18-0217.1.

Jou, B.J.-D. (2001) Introduction Green Island Mesoscale Experiment (GIMEX). *Quarterly Journal of Meteorology*, 167, 53–60 (in Chinese).

Jou, B.J.-D., Lee, W.-C. and Johnson, R.H. (2011) An overview of SOWMEX/TIMREX. In: Chang, C.-P., Ding, Y., Lau, N.-C., Johnson, R.H. and Yasunari, T. (Eds.) *The Global Monsoon*

System: Research and Forecast. Singapore: World Scientific, pp. 303–318. https://doi.org/10.1142/9789814343411_0018.

Kabasawa, M. (1950) Orographic precipitation of second kind: a case study. *Journal of Meteorological Research*, 2(3), 1–5 (in Japanese).

Ko, H.-C., Chun, H.-Y., Wilson, R. and Geller, M.A. (2019) Characteristics of atmospheric turbulence retrieved from high vertical-resolution radiosonde data in the United States. *Journal of Geophysical Research: Atmospheres*, 124(14), 7553–7579. https://doi.org/10.1029/2019JD030287.

Koike, M., Asano, N., Nakamura, H., Sakai, S., Nagao, T.M. and Nakajima, T.Y. (2016) Modulations of aerosol impacts on cloud microphysics induced by the warm Kuroshio current under the East Asian winter monsoon. *Journal of Geophysical Research: Atmospheres*, 121(20), 12282–12297. https://doi.org/10.1002/2016JD025375.

Koike, M., Takegawa, N., Moteki, N., Kondo, Y., Nakamura, H., Kita, K., Matsui, H., Oshima, N., Kajino, M. and Nakajima, T.Y. (2012) Measurements of regional-scale aerosol impacts on cloud microphysics over the East China Sea: possible influences of warm sea surface temperature over the Kuroshio ocean current. *Journal of Geophysical Research: Atmospheres*, 117(D17), D17205. https://doi.org/10.1029/2011JD017324.

Kuo, H.-C., Jou, B.J.-D., Yang, Y.-T. and Ong, H. (2017) The Taipei Summer Storm Experiment: introduction and preliminary results of 2016 pre-experiment. *Aviation Weather*, 27, 27–47 (in Chinese).

Kuo, Y.-H. and Chen, G.T.-J. (1990) The Taiwan Area Mesoscale Experiment (TAMEX): an overview. *Bulletin of the American Meteorological Society*, 71(4), 488–503 10.1175/1520-0477(1990)071<0488:TTAMEA>2.0.CO;2.

Lee, C.-W. and Chen, G.T.-J. (1983) Case study of heavy rainfall of 19 November 1980 over northern Taiwan. *Atmospheric Sciences*, 10(1), 25–38 (in Chinese with English abstract).

Lilly, D.K. (1968) Models of cloud-topped mixed layers under a strong inversion. *Quarterly Journal of the Royal Meteorological Society*, 94(401), 292–309. https://doi.org/10.1002/qj.49709440106.

Liu, J.-W., Xie, S.-P., Yang, S. and Zhang, S.-P. (2016) Low-cloud transitions across the Kuroshio front in the East China Sea. *Journal of Climate*, 29(12), 4429–4443. https://doi.org/10.1175/JCLI-D-15-0589.1.

Luce, H. and Hashiguchi, H. (2020) On the estimation of vertical air velocity and detection of atmospheric turbulence from the ascent rate of balloon soundings. *Atmospheric Measurement Techniques*, 13(4), 1989–1999. https://doi.org/10.5194/amt-13-1989-2020.

Maranan, M., Fink, A.H., Knippertz, P., Amekudzi, L.K., Atiah, W.A. and Stengel, M. (2020) A process-based validation of GPM IMERG and its sources using a mesoscale rain gauge network in the West African forest zone. *Journal of Hydrometeorology*, 21(4), 729–749. https://doi.org/10.1175/JHM-D-19-0257.1.

Nesbitt, S.W., Salio, P.V., Ávila, E., Bitzer, P., Carey, L., Chandrasekar, V., Deierling, W., Dominguez, F., Dillon, M.E., Garcia, C.M., Gochis, D., Goodman, S., Hence, D.A., Kosiba, K.A., Kumjian, M.R., Lang, T., Luna, L.M., Marquis, J., Marshall, R., McMurdie, L.A., de Lima Nascimento, E., Rasmussen, K.L., Roberts, R., Rowe, A.K., Ruiz, J.J., São Sabbas, E.F.M.T., Saulo, A.C., Schumacher, R.S., Skabar, Y.G., Toledo Machado, L.A., Trapp, R.J., Varble, A.C., Wilson, J., Wurman, J., Zipser, E.J., Arias, I., Bechis, H. and Grover, M.A. (2021) A storm safari in subtropical South America: Proyecto RELAMPAGO. *Bulletin of the American Meteorological Society*, 102(8), E1621–E1644. https://doi.org/10.1175/bams-d-20-0029.1.

Stephens, G.L. (2005) Cloud feedbacks in the climate system: a critical review. *Journal of Climate*, 18(2), 237–273. https://doi.org/10.1175/JCLI-3243.1.

Stephens, G.L. and Greenwald, T.J. (1991) The Earth's radiation budget and its relation to atmospheric hydrology: 2. Observations of cloud effects. *Journal of Geophysical Research: Atmospheres*, 96(D8), 15325–15340. https://doi.org/10.1029/91JD00972.

Takenaka, H., Sakashita, T., Higuchi, A. and Nakajima, T. (2020) Geolocation correction for geostationary satellite observations by a phase-only correlation method using a visible channel. *Remote Sensing*, 12(15), 2472. https://doi.org/10.3390/rs12152472.

Weckwerth, T.M. and Parsons, D.B. (2006) A review of convection initiation and motivation for IHOP_2002. *Monthly Weather Review*, 134(1), 5–22. https://doi.org/10.1175/mwr3067.1.

Wood, R. (2012) Stratocumulus clouds. *Monthly Weather Review*, 140(8), 2373–2423. https://doi.org/10.1175/mwr-d-11-00121.1.

Wu, C.-K. and Chen, J.-P. (2021) Simulation of aerosol indirect effects on cloud streets over the northwestern Pacific Ocean. *Journal of Geophysical Research: Atmospheres*, 126(11), e2020JD034325. https://doi.org/10.1029/2020JD034325.

Wu, C.-M., Lin, H.-C., Cheng, F.-Y. and Chien, M.-H. (2019) Implementation of the land surface processes into a vector vorticity equation model (VVM) to study its impact on afternoon thunderstorms over complex topography in Taiwan. *Asia-Pacific Journal of Atmospheric Sciences*, 55(4), 701–717. https://doi.org/10.1007/s13143-019-00116-x.

Wulfmeyer, V., Behrendt, A., Kottmeier, C., Corsmeier, U., Barthlott, C., Craig, G.C., Hagen, M., Althausen, D., Aoshima, F., Arpagaus, M., Bauer, H.-S., Bennett, L., Blyth, A., Brandau, C., Champollion, C., Crewell, S., Dick, G., Di Girolamo, P., Dorninger, M., Dufournet, Y., Eigenmann, R., Engelmann, R., Flamant, C., Foken, T., Gorgas, T., Grzeschik, M., Handwerker, J., Hauck, C., Höller, H., Junkermann, W., Kalthoff, N., Kiemle, C., Klink, S., König, M., Krauss, L., Long, C.N., Madonna, F., Mobbs, S., Neininger, B., Pal, S., Peters, G., Pigeon, G., Richard, E., Rotach, M.W., Russchenberg, H., Schwitalla, T., Smith, V., Steinacker, R., Trentmann, J., Turner, D.D., van Baelen, J., Vogt, S., Volkert, H., Weckwerth, T., Wernli, H., Wieser, A. and Wirth, M. (2011) The Convective and Orographically-induced Precipitation Study (COPS): the scientific strategy, the field phase, and research highlights. *Quarterly Journal of the Royal Meteorological Society*, 137(S1), 3–30. https://doi.org/10.1002/qj.752.

Yamamoto, Y., Ichii, K., Higuchi, A. and Takenaka, H. (2020) Geolocation accuracy assessment of Himawari-8/AHI imagery for application to terrestrial monitoring. *Remote Sensing*, 12(9), 1372. https://doi.org/10.3390/rs12091372.

How to cite this article: Su, S.-H., Chang, Y.-H., Liu, C.-H., Chen, W.-T., Chang, W.-Y., Chen, J.-P. *et al.* (2022) Observing severe precipitation near complex topography during the Yilan Experiment of Severe Rainfall in 2020 (YESR2020). *Quarterly Journal of the Royal Meteorological Society*, 1–20. Available from: https://doi.org/10.1002/qj.4271